



In situ synthesis of copper-modified graphene-reinforced aluminum nanocomposites with balanced strength and ductility

Jie Wang¹ , Xiang Zhang¹ , Naiqin Zhao^{1,2} , and Chunnian He^{1,2,*}

¹School of Materials Science and Engineering, Tianjin Key Laboratory of Composite and Functional Materials, Tianjin University, Tianjin 300072, China

²Collaborative Innovation Center of Chemical Science and Engineering, Tianjin 300072, China

Received: 11 September 2018

Accepted: 9 December 2018

Published online:
19 December 2018

© Springer Science+Business
Media, LLC, part of Springer
Nature 2018

ABSTRACT

In this work, a novel copper nanoparticles-modified graphene (Cu-NPs@GN)-reinforced Al matrix composites were fabricated. The Cu-NPs@GN hybrids were firstly synthesized by an NaCl template-assisted in situ CVD method and then incorporated into the Al matrix to fabricate Cu-NPs@GN/Al bulk composites by cold-press sintering and hot extrusion. With the merit of the unique characteristic of Cu-NPs@GN hybrid, the Cu-NPs@GN/Al composites exhibited homogeneously dispersed GNs and a strong GN–Al interfacial bonding. It was found that the in situ grown Cu-NPs@GN showed much better strengthening effect than that of the ex situ grown counterparts, which might be attributed to the pinning effect of Al₂Cu at the interface and thus promote the load transfer efficiency. Compared with pure Al, the composites with only 0.75 wt% Cu-NPs@GN exhibited a 68% increase in tensile strength (224 MPa) as well as had a total elongation of 17.5%.

Introduction

Metal matrix composites (MMCs) arise from the permanent demands for high-performance structural components in aerospace, automotive, electronic devices and military field [1, 2]. Among all the MMCs, aluminum matrix composites (AMCs) have attracted wide attention due to their lightweight but high strength [3]. However, aluminum matrix composites reinforced with traditional reinforcement

exhibit limitations and unsatisfactory comprehensive mechanical properties. Thus, new reinforcement materials possessing unique properties were developed for the further enhancement of mechanical properties of aluminum matrix composites [4–6]. Graphene, a single atomic layer carbon nanosheet, has recently attracted considerable attention due to its excellent mechanical, electrical and thermal properties [7]. Owing to its extraordinary mechanical properties such as high Young's modulus (1 TPa) and high tensile strength (130 GPa), graphene is

Address correspondence to E-mail: cnhe08@tju.edu.cn

considered to be an ideal reinforcement in Al matrix composites [8–11].

The research focused on graphene-reinforced Al matrix composites is still limited because there are several critical problems need to be resolved. One major issue is that it is hard to achieve uniform dispersion of graphene in the aluminum matrix due to its large specific surface area; in this case, the resulting aggregation of graphene would reduce its strengthen efficiency and even be harmful to the metal matrix [10]. To solve this issue, high-energy ball milling is often used to realize the uniform dispersion of graphene, but it is also accompanied by the destruction of graphene at the same time [12]. Another critical issue is the inherent poor wettability between graphene and metal matrix, which leads to a weak interfacial bonding during the consolidation process [13]. Therefore, fabricating graphene-reinforced Al matrix composites with uniformly dispersed graphene and intimate interfacial bonding simultaneously is still a great challenge.

It was reported that metal nanoparticles (MNPs) can be used as an interval to prevent the aggregation and restacking of graphene; meanwhile, the MNPs can form a chemical bonding between graphene and the metal matrix by alloying reaction during high-temperature consolidation process [14]. To further improve the interfacial bonding in MMCs, decorating or coating graphene with modification materials (metals [13], carbides [15], oxides [16]) to form a chemical bonding at the interface is considered to be an effective approach. Unfortunately, there are still few works concerning improving the wettability between graphene and metal matrix by surface modification. The existing work mainly focuses on decorating graphene with metal particles by an ex situ method (ball milling [17], chemical reduction [18], electroless plating [19]), which is very difficult to ensure the uniform distribution of MNPs and the tight coupling of MNPs/graphene. The MNPs loosely attached on the graphene surface are easy to fall off during the harsh mixing and consolidation processes; thus, the pinning effect of MNPs cannot be brought into full play. Therefore, in order to realize the uniform dispersion and the strong interfacial bonding in MMCs, the preparation of graphene decorated with MNPs by an in situ method still remains challenging. Our group firstly synthesized Ni NP-modified graphene-reinforced 6061Al composites by a simple NaCl-assisted in situ method, and

the interfacial bonding between graphene and 6061Al was significantly improved by Al₃Ni intermetallic [20]. However, the strengthening effect of Ni-NPs@GN is still unsatisfactory (30% enhancement for UTS), which may be attributed to the scarce existence of Al₃Ni. The Gibbs free energy of Al₂Cu formation is usually more negative than that of Al₃Ni formation at the same sintering temperature, indicating that the formation of Al₂Cu is more thermodynamically advantageous than that of Al₃Ni [21, 22]. Therefore, it can be supposed that using Cu NPs as an interfacial bonding agent would achieve better strengthening effect than Ni NPs.

Herein, an in situ synthesis strategy was proposed for preparing Cu NP-modified graphene hybrid (Cu-NPs@GN) -reinforced AMCs. With the merit of the spatial confinement function of NaCl template, a novel structure of Cu NPs tightly pinned on the graphene wall was firstly synthesized by in situ chemical vapor deposition (in situ CVD). Then, the Cu-NPs@GN powders were evenly dispersed in aluminum powder by a short time intermittent ball milling. Finally, the obtained composite powders were consolidated into a bulk by cold-press sintering and hot extrusion. The Cu NPs (~ 20 nm) anchored on graphene not only function as a catalyst for the in situ growth of high-quality graphene nanosheet (< 3 nm), but also facilitate the robust interfacial bonding between GN and Al matrix by forming Al₂Cu as a bridge. With only 0.75 wt% addition of reinforcement, the as-obtained Cu-NPs@GN-reinforced aluminum bulk exhibits a 68% enhancement for tensile strength compared with pure Al bulk. Furthermore, it is found that the in situ synthesized Cu-NPs@GN/Al has enhanced capabilities to better utilize the strengthening potential of graphene than the bulk composites reinforced with Cu@GN prepared by an ex situ method. To the best of our knowledge, this work demonstrates the most outstanding strengthening efficiency in modified graphene-reinforced AMCs. Moreover, the effects of Cu-modified graphene on the mechanical properties of the composites were illustrated, and the strengthening mechanisms were also discussed in detail.

Experimental

In situ synthesis of Cu-NPs@GN reinforcement powders

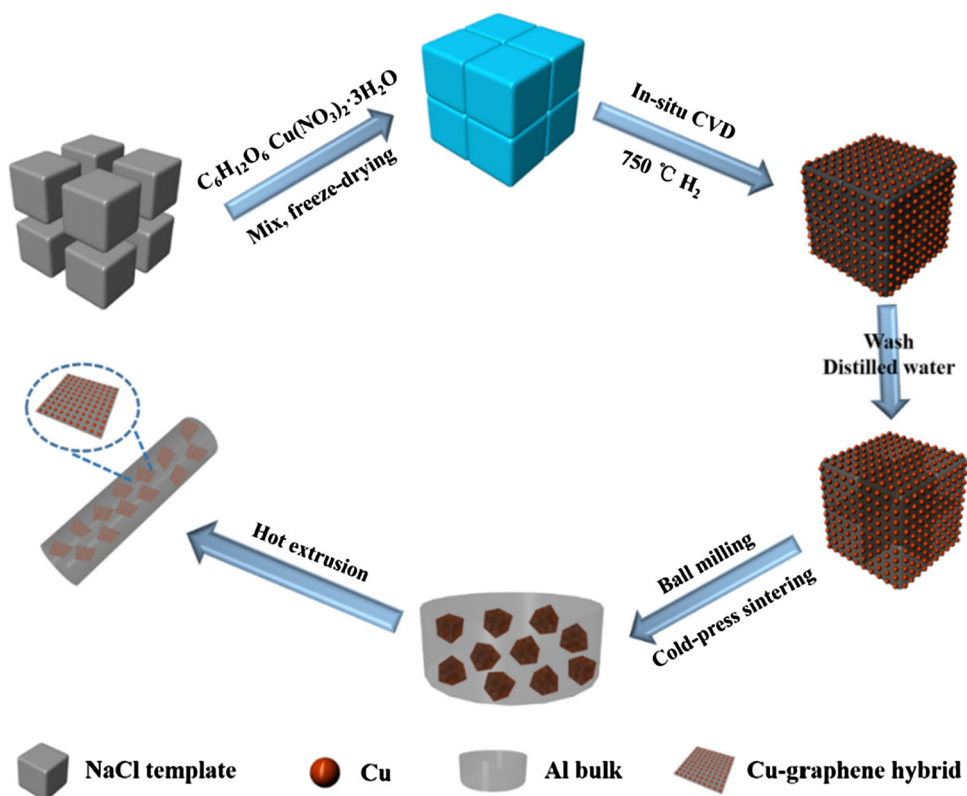
The overall production process is shown in Fig. 1. Firstly, Cu NPs decorated graphene hybrid (Cu-NPs@GN) powders were synthesized through our original NaCl template-assisted in situ CVD process [23, 24]. Typically, 2.265 g of $\text{Cu}(\text{NO}_3)_2 \cdot 3\text{H}_2\text{O}$, 0.938 g of anhydrous glucose and 36.590 g NaCl were dissolved in deionized water (120 mL) by magnetic stirring, and the obtained solution was frozen in a refrigerator at $-20\text{ }^\circ\text{C}$ for 24 h. Then, the water in the resulting gel is eliminated by freeze-drying and the obtained dry gel was ground to fine composite powders, which were further subjected to in situ CVD. During the in situ CVD process, 10-g powders placed inside the tube furnace were calcinated at $750\text{ }^\circ\text{C}$ for 2 h under H_2 and then cooled down to room temperature under Ar. The as-synthesized products were washed with deionized water several times to remove NaCl. After dried at $80\text{ }^\circ\text{C}$ in the oven overnight, pure Cu-NPs@GN powders were obtained. Pure Cu NPs and GN nanosheet were synthesized at the same preparation conditions just

without adding anhydrous glucose and $\text{Cu}(\text{NO}_3)_2 \cdot 3\text{H}_2\text{O}$ in precursor solution, respectively. For comparison, ex situ Cu/GN composites were prepared by hot-drying the solution of $\text{Cu}(\text{NO}_3)_2$ and pure GN, then the as-dried powders were reduced in a tube furnace under H_2 atmosphere. A simple blended mixture of pure GN nanosheet and Cu NPs were also prepared as a reference.

Synthesis of Cu-NPs@GN/Al composite powders

The second step is to incorporate Cu-NPs@GN into Al powder through a short time intermittent ball milling process in order to obtain uniform Cu-NPs@GN/Al composite powders. The Al powder ($\sim 10\text{ }\mu\text{m}$ in diameter) and Cu-NPs@GN were mixed in a stainless steel jar and milled for 90 min at a ball-to-powder ratio of 10:1 and a rotation speed of 360 rpm under the protection of Ar. To avoid the damage of graphene by heat concentration in continuous ball milling, the ball milling was paused for 30 min after every 10 min of milling. Stearic acid (0.2 wt%) was added as the process control agent to prevent the cold welding of aluminum powder.

Figure 1 Schematic illustration of the fabrication process of Cu-NPs@GN/Al bulk composites.



Fabrication of the Cu-NPs@GN/Al bulk composites

The Cu-NPs@GN/Al composite powders were added to a steel mold (20 mm in diameter) and then consolidated by cold-pressing under a pressure of 500 MPa. Then the obtained bulks were sintered at 630 °C for 1 h inside a tube furnace under Ar. To obtain a relatively high density, finer grain and GN well-dispersed materials, the as-sintered bulks were finally preheated to 550 °C and then subjected to hot extrusion with an extrusion ratio of 16:1 and a ram speed of 3 mm/s. The final Cu-NPs@GN/Al bulk composites were 5 mm in diameter, and the length could be controlled by the amount of powder added. Reference materials were also processed under the same route.

Characterization

Scanning electron microscopy (SEM, Hitachi S-4800) and transmission electron microscopy (TEM, JEOL JEM-2100F) were employed to view the microstructure of reinforcement powders and bulk composites. Raman spectroscopy (Renishaw, 532 nm Ar⁺ laser) was utilized to determine the quality of graphene. X-ray diffraction (XRD, Bruker D8 Advanced) was conducted using a Rigaku D/max diffractometer with Cu K α radiation at a wavelength of 1.5406 Å. Thermogravimetric analysis (TGA, Netzsch STA449f3) was used to determine the Cu or GN content in the Cu-NPs@GN composite powders. X-ray photoelectron spectroscopy (XPS) analysis of Cu-NPs@GN was performed on a PHI 1600 ESCA system using 300 W Al K α radiation. Electron backscattered diffraction (EBSD) analysis was conducted by using a HKL Channel 5 system to determine the average grain size of the bulk material. For tensile tests, the obtained bulk samples were machined on a lathe from an extruded rod to a dumbbell-like specimen with a gauge length of 17 mm and a diameter of 3 mm. Tensile tests were conducted on a CSS-44100 universal testing machine with a constant crosshead speed of 0.5 mm min⁻¹ at room temperature.

Results and discussion

Characterization of Cu-NPs@GN reinforcement

Generally, a novel in situ spatial confined synthesis strategy is adopted for preparing Cu-NPs@GN reinforcement with the assistance of water-soluble NaCl crystals, which is distinct from coating metal particles on graphene by an ex situ way like ball milling or chemical reduction. To be precise, the self-assembled NaCl crystals (Fig. 2a) can function as a template for the growth of graphene as well as restrain the agglomeration of Cu NPs due to the in situ spatial confinement effect generated from the self-assembly process [25, 26]. As illustrated in Fig. 1, self-assembled NaCl crystals coated with ultrathin composite film of Cu(NO₃)₂-C₆H₁₂O₆ were obtained by freeze-drying the homogeneous solution of Cu(NO₃)₂, C₆H₁₂O₆ and NaCl (see Fig. 2a), which were then subjected to in situ CVD. During the CVD process, the solid carbon source of C₆H₁₂O₆ was carbonized within the 2D-confined space between adjacent NaCl surfaces and further in situ catalyzed to graphene with the assistance of Cu NPs reduced from Cu(NO₃)₂ [23]. As a result, Cu-NPs@GN hybrids were obtained after removing the NaCl by distilled water. With the incorporation of dense Cu NPs on graphene, not only the serious agglomeration of graphene can be alleviated by using Cu NPs as a spacer, but also the poor wettability between aluminum and graphene can be improved by forming Al₂Cu at the interface.

The morphology of the in situ synthesized Cu-NPs@GN was characterized by SEM. As shown in Fig. 2b, the thin graphene framework with submicrometer-size well duplicates the space structure of the NaCl assembly. Dense Cu NPs (~ 20 nm) homogeneously and tightly anchored on the graphene walls are observed in high-magnification SEM images of Fig. 2c, while no aggregation of Cu NPs is found. Unlike the uniform distribution of Cu NPs on graphene in the Cu-NPs@GN, the Cu NPs in the ex situ Cu@GN prepared by impregnation-reduction process present a tendency to agglomerate into clusters (Fig. 2d) and are weakly attached on the surface of graphene, which verified the fatal drawback for the ex situ combination process of pre-synthesized GN and metal. Our group previously demonstrated that the in situ space-confined catalysis could suppress the overgrowth of metal NPs as well

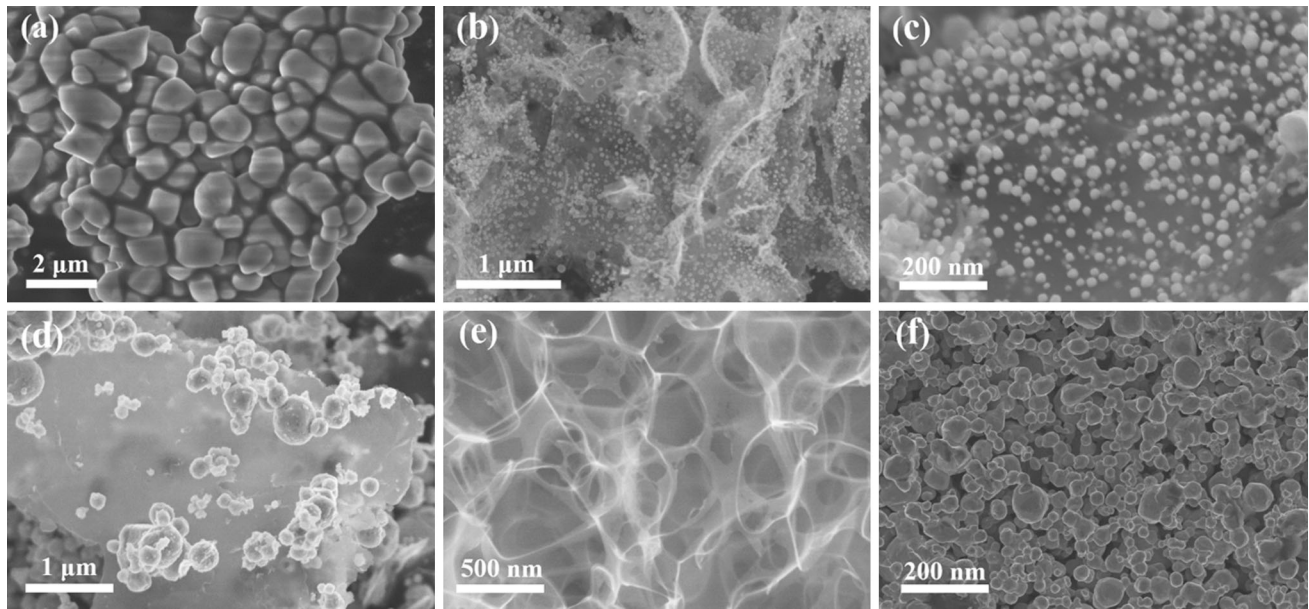


Figure 2 SEM images of **a** $\text{Cu}(\text{NO}_3)_2\text{-C}_6\text{H}_{12}\text{O}_6\text{@NaCl}$ precursor, **b, c** in situ Cu-NPs@GN , **d** ex situ Cu-NPs@GN , **e** pure GN nanosheet, **f** Cu NPs.

as guarantee the strong coupling between GN and metal [27], which is further confirmed in this work. Figure 2e, f demonstrates the typical SEM images of pure GN nanosheet and Cu NPs prepared by the same NaCl-assisted in situ CVD process, respectively. It can be seen that the Cu NPs were agglomerated into large particles when no carbon precursor were adopted.

TEM and high-resolution TEM (HRTEM) were employed to get insight into the microstructure of

Cu-NPs@GN . As shown in Fig. 3a and b, the graphene nanosheets were decorated with a mass of uniformly dispersed and firmly pinned Cu NPs (~ 20 nm), which facilitates the even distribution of graphene in aluminum powder during the subsequent mixing process as well as promotes the interfacial bonding between Al matrix and graphene in the consolidation process. In addition, it can be seen that the graphene walls exhibit transparent features, in good agreement with above SEM observations. It is

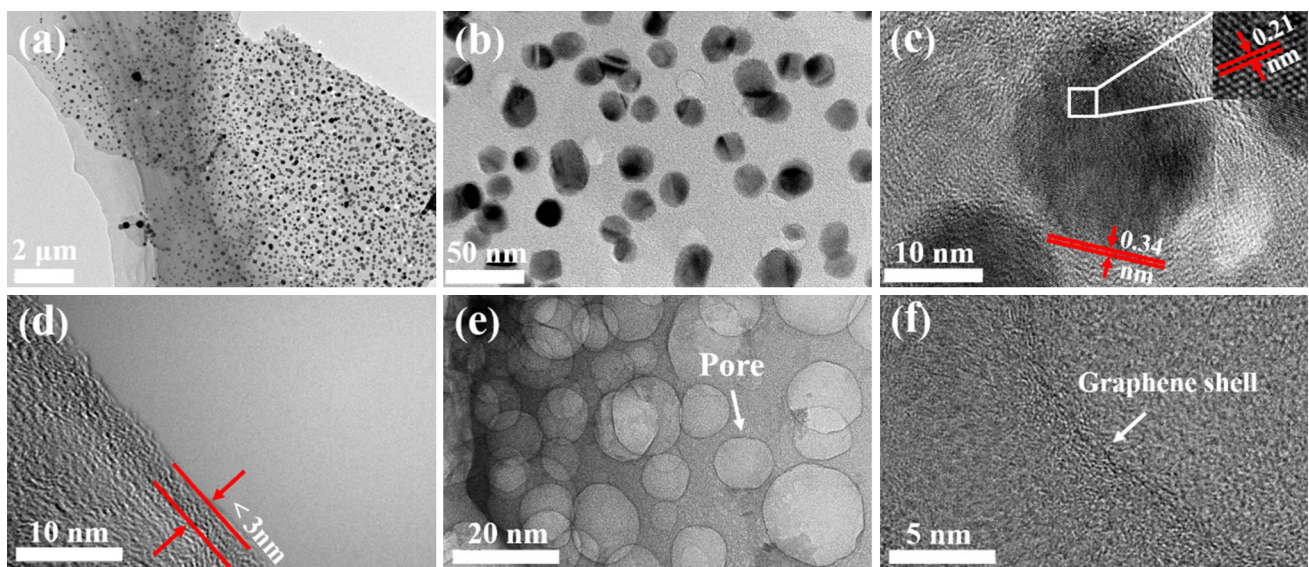


Figure 3 TEM images of **a, b** in situ Cu-NPs@GN , **c** typical Cu NP, **d** graphene layer, **e, f** pure GN nanosheet after etching Cu NPs.

noteworthy that the graphene network still remains intact and the Cu NPs are tightly anchored on graphene walls when subjected to intense ultra-sonication for 20 min during the preparation process of the TEM samples (see Fig. 3c), indicating an excellent mechanical features of graphene grown by CVD and a strong coupling of Cu NPs and graphene, which are very beneficial for the enhancement of the mechanical properties of the final bulk composites. According to Fig. 3c, the measured interplanar spacing of the graphene shells is ~ 0.34 nm, corresponding to (0 0 2) planes of graphite, while the lattice spacing of Cu NPs is ~ 0.21 nm, consistent with the (1 1 1) plane of Cu. Figure 3d depicts the edge of graphene wall with typical curved lattice fringes, the thickness of graphene is estimated to be less than 3 nm (< 10 layers). Many pores are observed on the graphene walls (Fig. 3e) after etching the Cu NPs from the Cu-NPs@GN, indicating that Cu NPs are partially embedded inside the GN walls instead of weak adsorption, which can be an evidence of Cu NPs tightly anchored on GN. Figure 3f exhibits the Cu NPs-catalyzed graphene shell around the pore, further validating an intimate interfacial bonding between GN and Cu NPs.

The crystallinity and quality of graphene in the Cu-NPs@GN powders were evaluated by Raman spectroscopy (Fig. 4a), which clearly reveals typical D (1335 cm^{-1}), G (1570 cm^{-1}) and 2D (2670 cm^{-1}) peaks of graphene. The intensity ratios of the D-band to the G-band (I_D/I_G) and the 2D-band to the G-band (I_{2D}/I_G) of the composite powders are calculated to be 0.92 and 0.40, respectively. The lower relative intensity of the D-band peak and the sharp 2D-band reveal the relatively high crystallinity of few-layered graphene in the composite powders. On the basis of TGA (Fig. 4b), the original contents of Cu in the

in situ Cu-NPs@GN and ex situ Cu-NPs@GN are calculated to be 80 and 79 wt%, respectively. This result verifies that the in situ Cu-NPs@GN and ex situ Cu-NPs@GN possess almost identical composition, which facilitates the later comparison of their mechanical properties. The phase composition of the Cu-NPs@GN detected by XRD is shown in Fig. S1. Three sharp diffraction peaks at 43.5° , 50.4° , and 74.0° correspond to Cu (111), (200), (220) lattice plane (PDF#01-1241), respectively. Considering the heavy loading of Cu on graphene (80 wt%), the diffraction peak of graphene is relatively weak due to the strong interference of Cu metallic phase [13, 19]. XPS analysis in Fig. 4c reveals the strong C=C (sp^2 284.7 eV) peaks for Cu-NPs@GN, further indicating the well-crystallized GNs of Cu-NPs@GN [28].

Characterization of Cu-NPs@GN/Al bulk composites

Figure 5a displays the XRD pattern of the Cu-NPs@GN/Al bulk composites after hot extrusion. It is worth noting that obvious sharp diffraction peaks emerge at the angle of 20.6° , 29.4° , 42.1° , 42.6° , 47.3° and 47.8° in the Cu-NPs@GN/Al bulk composites, attributing to Al_2Cu (110), (200), (220), (112), (310) and (202) lattice plane (PDF#25-0012), respectively. Strong diffraction peaks of Al_2Cu demonstrate the presence of chemical bonding between aluminum and Cu NPs, which can be inferred that the Al_2Cu plays a role in bridging aluminum and graphene at the interface. Figure 5b–e depicts the element mapping images of the bulk composite. No obvious element accumulation can be found in the bulk composite, further confirming the uniform distribution of Cu-NPs@GNP in the composites.

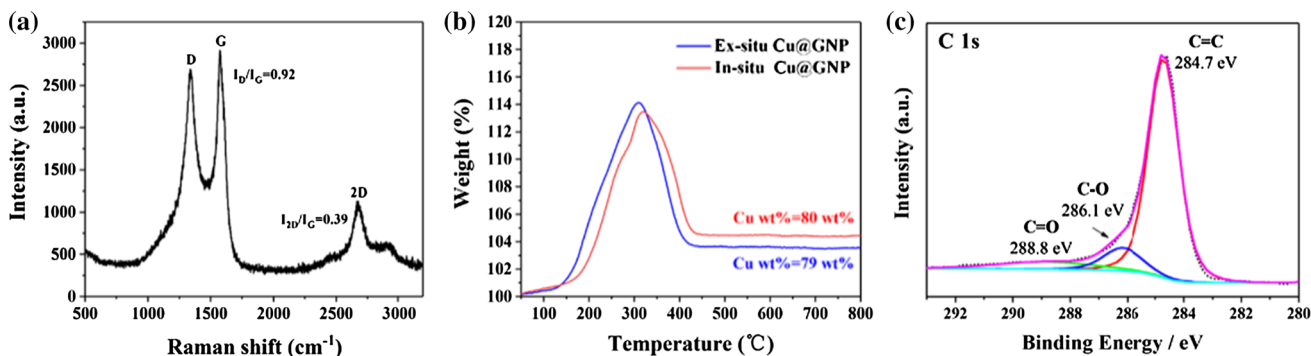


Figure 4 a Raman spectrum, b TGA profile, c C 1s spectrum of Cu-NPs@GN.

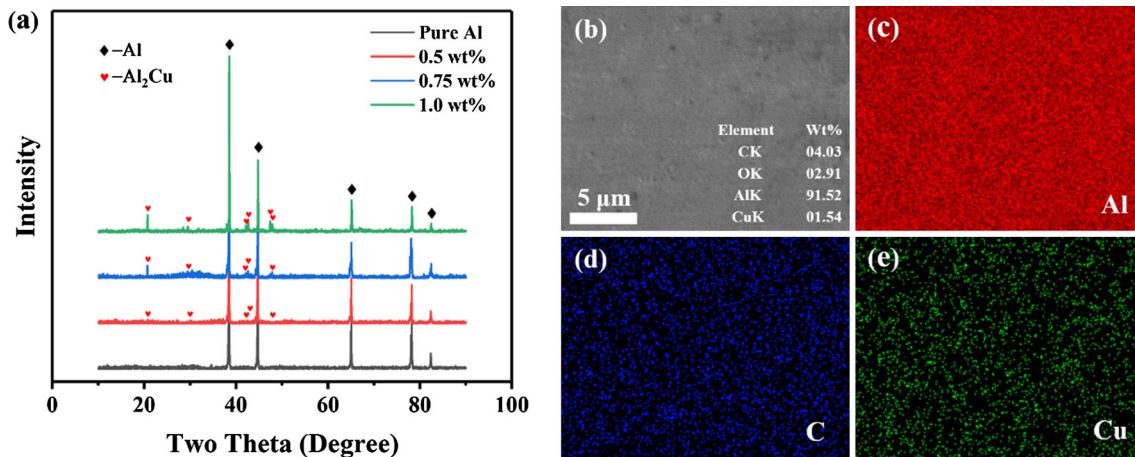
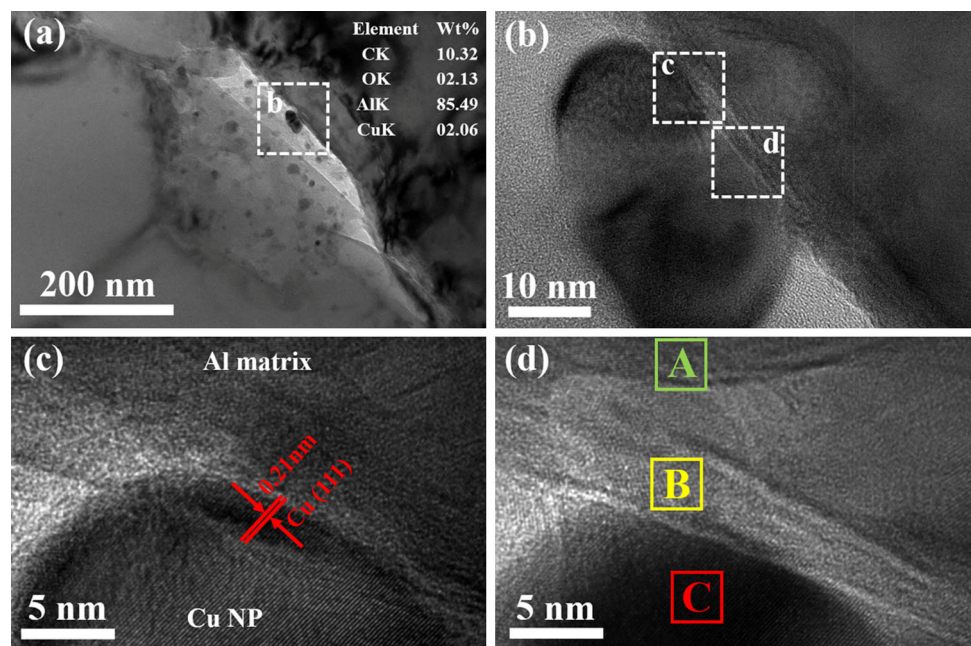


Figure 5 a XRD patterns, b–e EDS mapping images of in situ Cu-NPs@GN/Al bulk composites after hot extrusion.

TEM micrograph perpendicular to in-plane of GNs was utilized to gain insight into the distribution and microstructure of Cu-NPs@GN in the Al matrix. According to Fig. 6a, the light-colored flaky phases appear at the boundary of several grains, which is confirmed to be Cu-NPs@GN by EDS results shown in insets. Cu-NPs@GN with a large size and a dense Cu NPs anchored on it still remains intact after the harsh milling, sintering and hot extrusion process, further revealing the excellent mechanical flexibility of graphene and a robust bonding between Cu NPs and graphene nanosheet. Figure 6b depicts the clear and unseamed interface (indicated by white square in Fig. 6b) between Al and graphene, which clearly

shows that Cu NPs were located at the interface. Moreover, part of some Cu NP penetrates into the interior of the aluminum matrix, validating that the Cu NPs play the role of bridging aluminum matrix and graphene at the interface (see Fig. 6c). It is well known that there is little wettability between graphene and aluminum, and the wettability between aluminum and copper is more favorable [13]. With the infiltration of copper atoms into aluminum matrix during high-temperature processing, the poor wettability between aluminum and graphene can be effectively improved by the copper atom as an interfacial bonding agent. To better comprehend the interfacial characteristics of bulk composites, the

Figure 6 a TEM images of the 0.75 wt% Cu-NPs@GN bulk materials, b magnification of the interface in the composites. c and d are the corresponding magnification of the selected area in (b), respectively.



interface of Al-Cu-NPs@GN was characterized by EDS analysis (see Fig. S2) [3]. The chemical composition variations near the interface indicate the possible existence of Al₂Cu intermetallic (related discussions were concluded in Supplementary data).

Figure 6d presents a typical chemical interfacial bonding at nanoscale; the substance in each region is determined by measuring interplanar spacing together with diffraction analysis. The details of interface analysis are shown in Fig. 7. Region A is the metal matrix, the measured d-spacing of 0.143 nm should be corresponding to the (220) Al; Region B represent the Cu NP anchored on the GN; the measured interplanar spacing of 0.186 nm could be ascribed to the (200) Cu; Region C is the junction area of aluminum matrix and Cu NP, and the measured d-spacing of 0.306 nm corresponds to (200) Al₂Cu. Considering the solid interfacial bonding between Cu NPs and graphene, the existence of Al₂Cu at the

interface indicates the strong chemical bonding between aluminum and graphene, well consistent with the results of XRD analysis. The interface between GN and metal matrix is demonstrated as the mode of Al-Al₂Cu-Cu@GN, and the interfacial strength can be greatly promoted by forming Al₂Cu intermetallic compound as a “rivet.”

In order to further determine the effect of Cu NPs on the bridging of aluminum and graphene, Al matrix in the Cu-NPs@GN/Al bulk composites was completely etched by Keller’s corrodent, and the remaining graphene is characterized by scanning TEM (STEM) after several times of washing and centrifuging. Fig. S3 depicts the EDS mapping of remaining graphene, and it can be clearly seen that a large amount of Cu element and Al element are distributed on the carbon matrix. It is noteworthy that the position of Al element and Cu element is almost exactly overlapping on graphene, while there is no

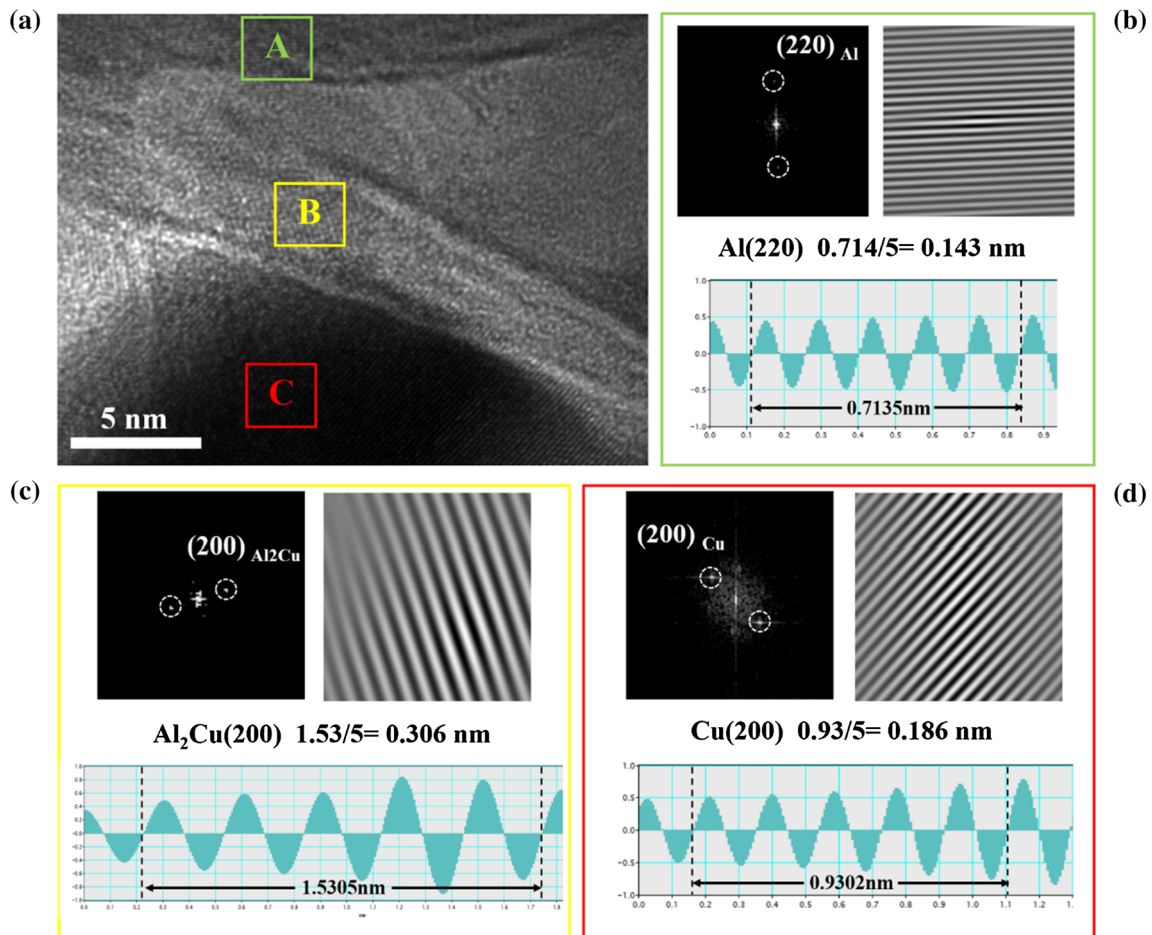


Figure 7 HRTEM images and microstructure analysis of the interfacial bonding area in Fig. 6d. **a** Interface, **b–d** corresponding magnification of the selected area in (a), respectively.

existence of Al element in the region without Cu element. Since Al has been fully removed by Keller's corroder, we can conclude that Al element and Cu element on graphene mostly exist in the form of Cu and Al₂Cu. The results of STEM perfectly agree with the above XRD and TEM observations, that is, Cu plays a bridging role between aluminum and graphene through the formation of the Al₂Cu. The chemical bonding instead of mechanical bonding significantly enhances the interfacial bonding between graphene and aluminum, thereby avoiding the interfacial slip between graphene and aluminum under external loading, thus further improving the mechanical properties of the final bulk composites.

Mechanical properties of the Cu-NPs@GN/Al bulk composites

The mechanical properties of the Cu-NPs@GN/Al bulk composites with various graphene contents are demonstrated in Table 1. The representative engineering tensile stress–strain curves of the Cu-NPs@GN/Al bulk composites are depicted in Fig. 8a. The Cu-NPs@GN/Al composite with only 0.5 wt% Cu-NPs@GN content is shown to have a yield strength of 121 MPa and a tensile strength of 191 MPa, ~ 51.3% and ~ 43.3% higher than that of the pure Al matrix fabricated through the identical processing routes, respectively. When the content of Cu-NPs@GN is increased to 0.75 wt%, the yield strength and tensile strength of the composite reach the maximum 140 MPa and 223 MPa, respectively (75% and 68% higher than that of the pure Al matrix). Compared to our previous work of Ni-modified graphene-reinforced 6061Al matrix composites, Cu-NPs@GN exhibited a much better strengthening effect on the tensile strength (Ni@GN/Al shows only 30% enhancement for tensile strength). The better strengthening effect of Cu-NPs@GN may be attributed to the fact that the Cu NPs are more capable to play the role of interface bridging since Al is prone to

react with Cu to form Al₂Cu intermetallic, making it possible for Cu-NPs@GN to fully exert its load-bearing capability. However, with the increasing addition of Cu-NPs@GN up to 1.0 wt%, the yield strength and tensile strength of the Cu-NPs@GN/Al fall down to 125 MPa and 201 MPa, respectively. This may be attributed to the common issue that high content of graphene is hard to disperse homogeneously in aluminum matrix, and thus, the resulting agglomeration of graphene is detrimental to the mechanical properties of the bulk composites [10, 20].

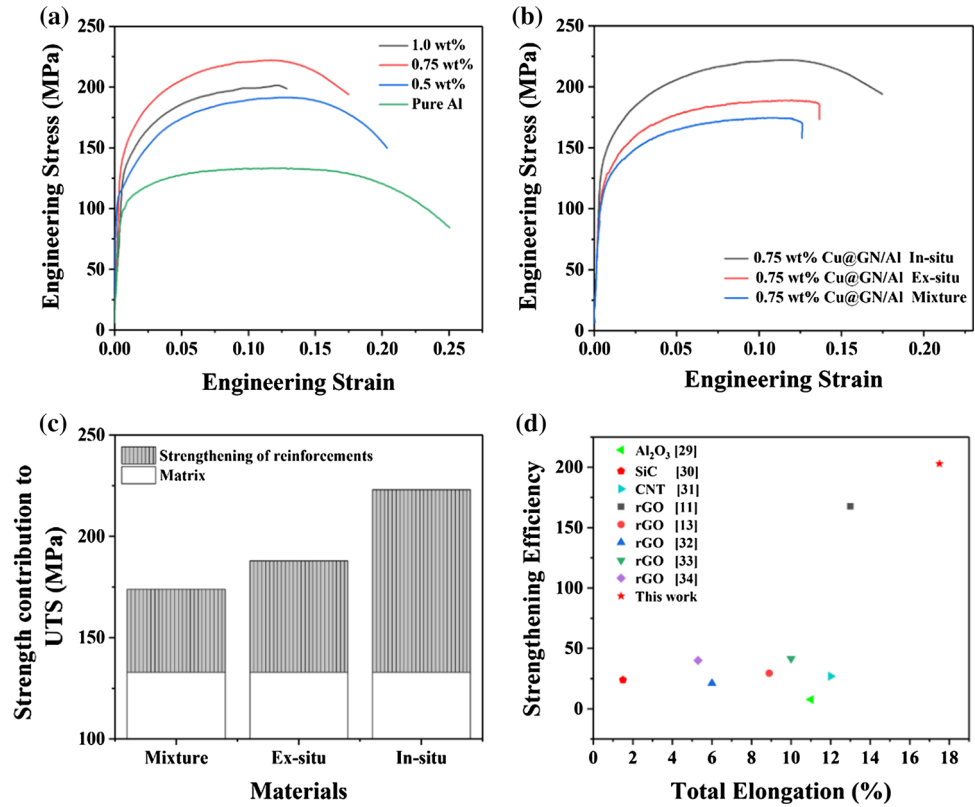
It is well known that the appearance of necking is the result of the plastic deformation of the material. The obvious necking stage in the Cu-NPs@GN/Al composites manifests that the final bulk material possesses an excellent plastic deformation capability. The total elongation of the Cu-NPs@GN/Al composite (20.3% and 17.5% for composites containing 0.5 wt% and 0.75 wt% Cu-NPs@GN content, respectively) is moderately lower than that of the pure Al matrix (25.2%). Considering the loss of ductility after hot extrusion, the elongation of 17.5% is still far more satisfactory for the critical ductility (5%) required for many structural applications [29]. The outstanding ductility of the Cu-NPs@GN/Al composites may be due to the intimate interfacial bonding between GN and Al matrix, together with the unique graphene network structure containing a lot of wrinkles generated by template of NaCl (Fig. 2b). When the composite is deformed, the Cu-NPs@GN tightly pinned on the Al matrix can be stretched into a plane surface and further pulled out, which can effectively inhibit the crack propagation and final failure of the composite, and thus, the toughness of the Al matrix can be preserved to a large extent.

Tensile curves of ex situ Cu@GN/Al and mixed Cu@GN/Al are shown in Fig. 8b. It can be seen clearly that the in situ Cu@GN/Al possesses superior strength and ductility than ex situ counterpart, while the mixture of Cu/GN-reinforced Al exhibits the

Table 1 Mechanical properties of Al matrix composites reinforced by in situ Cu-NPs@GN

Reinforcement content (wt%)	Yield strength (MPa)	Tensile strength (MPa)	Total elongation (%)	Microhardness (HV)
0	80.5 ± 3.7	133.4 ± 3.2	25.2 ± 0.3	85.1 ± 2.2
0.5	121.3 ± 3.3 (+51%)	189.9 ± 2.4 (+42%)	20.3 ± 0.4	102.1 ± 4.1
0.75	140.2 ± 2.4 (+75%)	223.5 ± 5.6 (+68%)	17.5 ± 1.1	123.4 ± 5.6
1.0	125.5 ± 2.4 (+56%)	201.3 ± 3.3 (+51%)	12.8 ± 1.3	109.3 ± 4.2

Figure 8 **a** Stress–strain curves of Al and composites reinforced by various content of in situ Cu-NPs@GN. **b** Stress–strain curves of composites reinforced by in situ, ex situ and mixture of Cu-NPs@GN. **c** Strength contribution to UTS of different reinforcements. **d** Comparison of strengthening efficiency versus total elongation of Al matrix composites reinforced by different types of reinforcements.



worst mechanical properties. Since the composition of different reinforcement is almost identical, the variation of mechanical properties may be attributed to the different interfacial bonding state of composites. The Cu NPs tightly anchored on in situ Cu/GN can still maintain during the consolidation process, while the Cu NPs weakly attached on GN nanosheet by an ex situ method could easily fall off during the same process. It is clarified that the Cu NPs play an important role on bridging graphene and Al matrix; thus, the strengthening effect of the in situ Cu-NP@GN surpass the ex situ contrast as well as the simple mixture of each component. Figure 8c demonstrates the strength contribution to UTS with different type of reinforcements, and the UTS contribution of in situ Cu-NPs@Al is 90.1 MPa, which is much higher than ex situ counterpart (45.7 MPa) and mixture of Cu/GN (36.6 MPa).

The strengthening efficiency R is adopted to evaluate the strengthening capability of reinforcement in Al matrix composites, which is defined as the strength enhancement per unit volume fraction of the reinforcement. The strengthening efficiency R of the reinforcement can be expressed as below:

$$R = (\sigma_c - \sigma_m) / V_f \sigma_m$$

where σ_c is tensile strength of the composite, σ_m is the tensile strength of the matrix and V_f is the volume fraction of the reinforcement. For the correct comparison of normalizing purposes, all the references in Fig. 8d are chosen and compared based on pure Al matrix composites. The mass fraction of the reinforcement in all references is converted into volume fraction by assuming that the compact density of graphene and aluminum is 2.2 g/cm³ and 2.7 g/cm³, respectively. By the result of the TGA, we can calculate that the theoretical compact density of our Cu-NPs@GN is 6.16 g/cm³; thus, the mass fraction of 0.75 wt % is corresponding to the volume fraction of 0.33 vol%. As shown in Fig. 8d, the strengthening efficiency (R) of 0.75 wt% Cu-NPs@GN/Al composite is calculated to be 203, which is considerably higher than those of previously reported pure Al matrix composites reinforced by other reinforcements, such as Al₂O₃ [29], SiC [30], CNT [31], rGO [11, 13, 32–34]. (The detailed discussion and comparison of strengthening and toughening mechanism with reported works were presented in the Supplementary data.) The outstanding strengthening efficiency and relatively high elongation of Cu-NPs@GN/Al composite demonstrate that our Cu-NPs@GN is a

promising reinforcement for Al matrix composites requiring high strength and high ductility.

Fracture mechanism analysis

The microstructure analysis of the fractured samples of the pure Al bulk and Cu-NPs@GN/Al bulk composite are shown in Fig. 9. It can be seen clearly that pure Al bulk possesses many deep and broadened dimples after tensile fracture, demonstrating a typical ductile failure. Comparing with pure Al bulk, 0.75 wt% Cu-NPs@GN/Al bulk composite shows a fewer and shallower dimple fracture morphology, which is well consistent with the ductility variations. The pulled out Cu-NPs@GN were observed at the fractured surface of the bulk composite (as marked with circles in Fig. 9d), validating the excellent load-bearing effect of graphene derived from the tight interfacial bonding. This result suggests that the Cu-NPs@GN hybrid facilitates the robust interfacial bonding between Al matrix and graphene and thus guarantees the load transfer strengthen capability of graphene to be exert efficiently.

Strengthening mechanisms

Generally, load transfer, grain refinement, Orowan strengthening and thermal mismatch are commonly regarded as the four kinds of mechanisms for the strengthening of graphene-reinforced metal

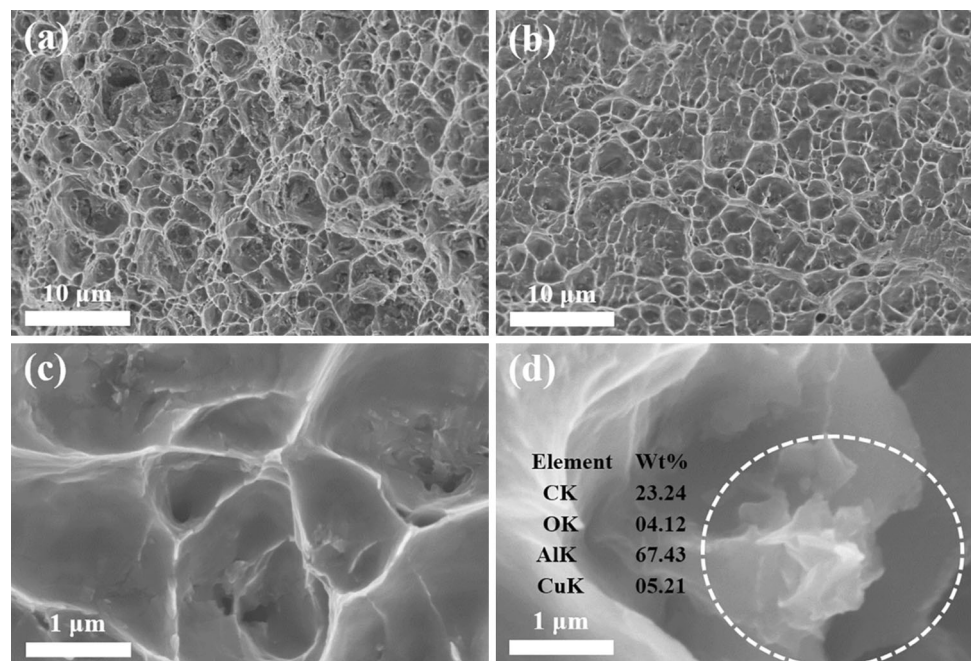
composites [35, 36]. It is noteworthy that the pile-up of dislocations caused by thermal mismatch only occurs when composites are undergoing fast cooling such as quenching, which is not suitable for slow air-cooled composites after hot extrusion [37]. Therefore, thermal mismatch strengthening associated with the different thermal expansion coefficients between reinforcement and matrix should be less considered in present case. As a consequence, the strengthening effect of reinforcement can be expressed as the combination of the three possible strengthening mechanisms, which could be written as below:

$$\sigma_c = \sigma_m + \Delta\sigma_{LT} + \Delta\sigma_{GR} + \Delta\sigma_{OR}$$

where σ_c and σ_m are the tensile strength of composite and matrix, respectively. $\Delta\sigma_{LT}$, $\Delta\sigma_{GR}$, $\Delta\sigma_{OR}$ represent the strengthening effect of load transfer, grain refinement and Orowan looping, respectively.

The grain information of the Al bulk and Cu-NPs@GN/Al bulk composites was investigated to verify the grain refinement effect by EBSD analysis (Fig. 10 and Fig. S4). Figure 10 demonstrates the grain information of pure Al and 0.75 wt% in situ Cu-NPs@GN/Al. The pure Al bulk has a uniform grain distribution with an average grain size of 2.88 μm (Fig. 10a, b). The average grain size was decreased to 1.58 μm for the 0.75 wt% Cu-NPs@GN/Al bulk composites (Fig. 10c, d), indicating that the grain size of Al matrix composites was obviously refined after

Figure 9 SEM image of the fractured surface of **a, c** pure Al and **b, d** 0.75 wt% in situ Cu-NPs@GN/Al bulk composites.



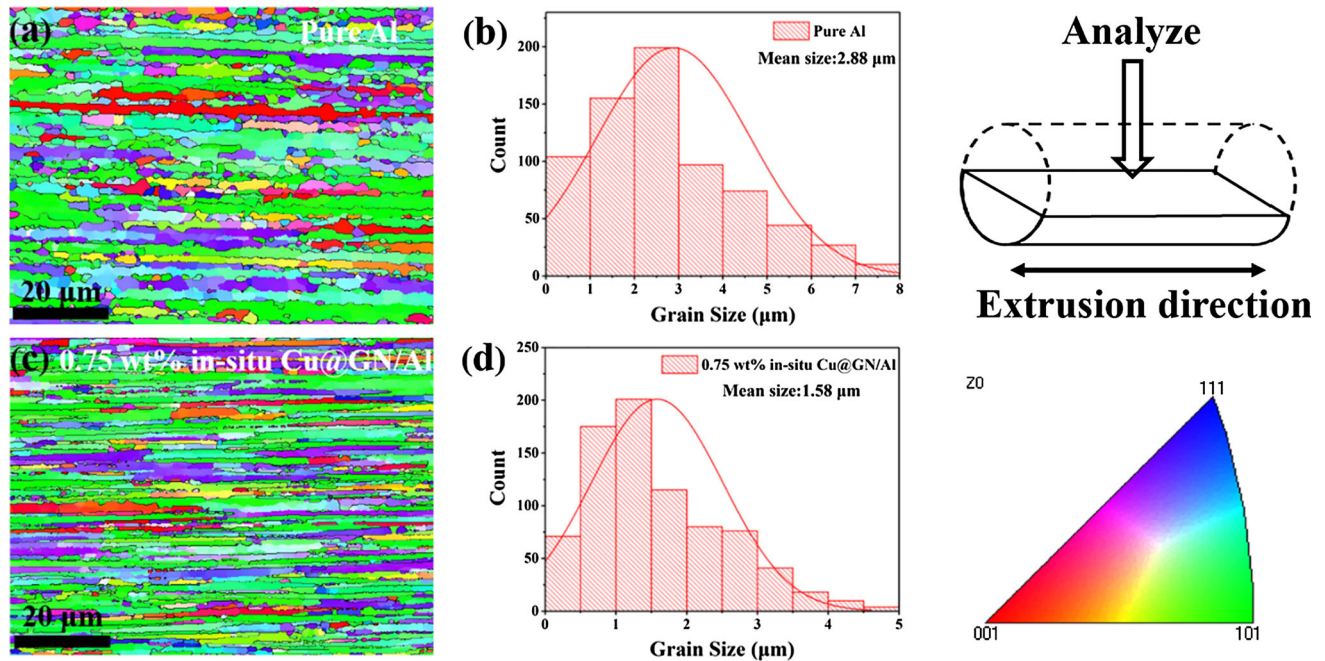


Figure 10 Grain information of pure Al and AMCs measured by EBSD. **a, b** Pure Al, **c, d** 0.75 wt% in situ Cu-NPs@GN/Al.

adding GNs. Grain refinement is directly attributed to grain growth stagnation with the addition of GNs, which inhibits the growth of Al grains during consolidation process [38]. The strength contribution of grain refinement ($\Delta\sigma_{GR}$) can be calculated based on Hall–Patch relationship [39]:

$$\Delta\sigma_{GR} = K(d_c^{-0.5} - d_m^{-0.5})$$

where K is a constant (0.04 MPa $m^{0.5}$ for Al [37]), d_c and d_m are the average grain sizes for the composite and pure Al, respectively. According to the grain size of the samples measured by EBSD, $\Delta\sigma_{GR}$ is calculated and listed in Table 2.

Orowan strengthening is frequently ignored for graphene-reinforced MMCs due to the inherent large surface area of graphene [40]. However, it is known that ultrafine NPs inserted in the metal matrix strengthen the composite by way of Orowan looping [37]. The Cu NPs uniformly distributed in Al matrix

may accumulate to hinder dislocation propagation and form Orowan loops in this case. The presence of Cu NPs insertion in Al grain was shown in Fig. 6c, and the Orowan loops were found in Al matrix (Fig. S5); thus, the impact of Orowan strengthening should be taken into account in this case. The strength contribution of Orowan strengthening ($\Delta\sigma_{OR}$) can be determined by the given Orowan–Ashby equation [41]:

$$\Delta\sigma_{OR} = \frac{M G b}{2.36 \pi} \cdot \ln\left(\frac{\phi}{2b}\right) \cdot \frac{1}{\lambda - \phi}$$

where M is the Taylor factor (3.06 for face-centered cubic metals such as Al [40]), G is the shear modulus (25.4 GPa for Al [37]), b is the magnitude of the Burgers vector (0.286 nm for Al [37]), ϕ is the nanoparticle diameter (~ 20 nm for Cu NPs, Fig. 3b) and λ is the inter-particle spacing, which can be

Table 2 Strengthening factors of Al matrix composites reinforced by Cu-NPs@GN

Reinforcement content (wt%)	Grain refinement (MPa)	Orowan strengthening by Cu (MPa)	Load transfer by GN (MPa)
0.50 (in situ)	5.4 (9.6%)	16.2 (28.7%)	34.9 (61.7%)
0.75 (in situ)	8.3 (9%)	20.7 (23%)	61.1 (68%)
1.00 (in situ)	6.2 (9.1%)	23 (33.9%)	38.7 (57%)
0.75 (mixed)	5 (11.9%)	20.7 (49.3%)	16.3 (38.8%)

calculated by assuming Cu NPs are evenly dispersed in the Al matrix (Fig. 5e) [40]:

$$\lambda = \frac{1}{2} \phi \sqrt{\frac{3\pi}{2V_{Cu}}} \quad (1)$$

where V_{Cu} is the volume fraction of Cu NPs. The strength contribution of Orowan strengthening is calculated and listed in Table 2.

It is generally accepted that the strengthening effect of graphene-reinforced composites is mainly depending on the load transfer from matrix to graphene. Considering the large surface area of graphene nanosheet, robust interfacial bonding between matrix and graphene is crucial for improving the load transfer efficiency [34, 38, 42]. The contribution of load transfer is hard to quantify by direct equations in present case, but it could be determined as $\Delta\sigma_{LT} = \sigma_c - \sigma_m - \Delta\sigma_{GR} - \Delta\sigma_{OR}$ according to Eq. (1).

The strengthening factors ($\Delta\sigma_{LT}$, $\Delta\sigma_{GR}$ and $\Delta\sigma_{OR}$) for Cu-NPs@GN/Al composites are listed in Table 2 and summarized in Fig. 11. It can be seen that grain refinement (8.3 MPa) and Orowan strengthening (20.7 MPa) moderately contributed to the total strength. Obviously, the load transfer (61.1 MPa) dominated the main strengthening contribution ($\sim 68\%$ proportion) for the 0.75 wt % Cu-NPs@GN/Al composite. Moreover, the $\Delta\sigma_{LT}$ of the 0.75 wt% in situ Cu-NPs@GN/Al bulk is 275% larger than that of Cu-GN mixture/Al bulk, demonstrating a superior load-bearing ability of GN in the in situ Cu-NPs@GN/Al composite. As illustrated in Fig. S6, the

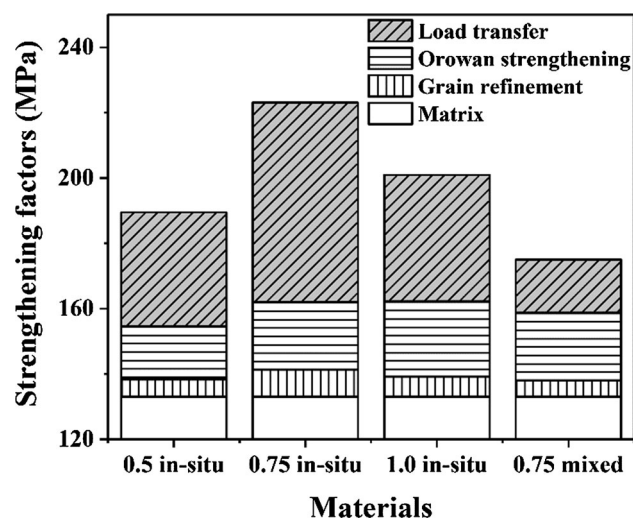


Figure 11 Strengthening factors in Cu-NPs@GN/Al composites.

in situ synthesized Cu-NPs@GN guarantees excellent chemical bonding between matrix and graphene instead of poor mechanical bonding by forming Al_2Cu intermetallic at the interface, which is confirmed by XRD analysis and TEM observations. The mechanical property measurements demonstrate that the in situ synthesized Cu-NPs@GN shows a better strengthening effect than ex situ synthesized Cu-NPs@GN as well as simple mixture of Cu NPs and graphene; this may also attribute to excellent interfacial bonding state of in situ Cu-NPs@GN/Al. The pull-out and breaking of GN during AMC deformation can be inhibited or delayed by Al_2Cu intermetallic compounds distributed near the interface. The Al_2Cu intermetallic distributed near the interface can be exploited to inhibit or delay the pull-out and breaking of GNs during deformation process; thus, the load transfer efficiency can be promoted and the inherent ultrahigh strength of GNs can be fully exerted. These results confirm the dual function of Cu NPs that not only significantly improve the load transfer efficiency by forming Al_2Cu at interface but also play a role of the possible Orowan strengthening themselves.

Conclusions

In summary, the Cu-NPs@GN/Al composites with uniformly distributed GN and strong interfacial bonding have been successfully fabricated through cold-press sintering followed by hot extrusion. The Cu-NPs@GN synthesized by in situ CVD process has tightly anchored Cu NPs on the surface of graphene, which facilitates the uniform dispersion of GN and intimate interfacial bonding between GN and metal matrix during the mixing and consolidation process. The interface between GN and metal matrix is demonstrated as the mode of Al- Al_2Cu -Cu@GN, which greatly promoted the interfacial load transfer efficiency by forming Al_2Cu intermetallic compound as a “rivet.” The tensile strength of the Cu-NPs@GN/Al composite improved by $\sim 68\%$ with the addition of 0.75 wt% Cu-NPs@GN and without the sacrificing of the total elongation. Improved mechanical properties were mainly attributed to the load transfer and grain refinement in our Cu-NPs@GN/Al composites. This novel modification strategy may open up a new avenue to optimize the interface bonding toward

fabricating advanced graphene/metal composites with excellent comprehensive properties.

Acknowledgements

The authors gratefully acknowledge the financial support by the National Natural Science Funds for Excellent Young Scholar (Grant No. 51422104), the National Natural Science Foundation of China (Grant Nos. 51531004, 51771130 and 51472177), the Tianjin Youth Talent Support Program, the Tianjin Natural Science Funds for Distinguished Young (Grant No. 17JCJQC44300) and the Tianjin Science and Technology Support Project (Grant No. 17ZXCLGX00060).

Electronic supplementary material: The online version of this article (<https://doi.org/10.1007/s10853-018-03245-2>) contains supplementary material, which is available to authorized users.

References

- [1] Rabadia CD, Liu YJ, Wang L et al (2018) Laves phase precipitation in Ti–Zr–Fe–Cr alloys with high strength and large plasticity. *Mater Des* 154:228–238
- [2] Ehtemam-Haghighi S, Liu Y, Cao G et al (2016) Influence of Nb on the $\beta \rightarrow \alpha$ martensitic phase transformation and properties of the newly designed Ti–Fe–Nb alloys. *Mater Sci Eng C Mater Biol Appl* 60:503–510
- [3] Yu P, Zhang LC, Zhang WY et al (2007) Interfacial reaction during the fabrication of Ni₆₀Nb₄₀ metallic glass particles-reinforced Al based MMCs. *Mater Sci Eng, A* 444:206–213
- [4] Zhou W, Yamaguchi T, Kikuchi K et al (2017) Effectively enhanced load transfer by interfacial reactions in multi-walled carbon nanotube reinforced Al matrix composites. *Acta Mater* 125:369–376
- [5] Zhao M, Xiong DB, Tan Z et al (2017) Lateral size effect of graphene on mechanical properties of aluminum matrix nanolaminated composites. *Scripta Mater* 139:44–48
- [6] Feng S, Guo Q, Li Z et al (2017) Strengthening and toughening mechanisms in graphene–Al nanolaminated composite micro-pillars. *Acta Mater* 125:98–108
- [7] Lee C, Wei X, Kysar JW et al (2008) Measurement of the elastic properties and intrinsic strength of monolayer graphene. *Science* 321:385–388
- [8] Chen SJ, Li CY, Wang Q et al (2017) Reinforcing mechanism of graphene at atomic level: friction, crack surface adhesion and 2D geometry. *Carbon* 114:557–565
- [9] Shin SE, Choi HJ, Shin JH et al (2015) Strengthening behavior of few-layered graphene/aluminum composites. *Carbon* 82:143–151
- [10] Yan SJ, Dai SL, Zhang XY et al (2014) Investigating aluminum alloy reinforced by graphene nanoflakes. *Mater Sci Eng, A* 612:440–444
- [11] Wang J, Li Z, Fan G et al (2012) Reinforcement with graphene nanosheets in aluminum matrix composites. *Scr Mater* 66:594–597
- [12] Bartolucci SF, Paras J, Rafiee MA et al (2011) Graphene–aluminum nanocomposites. *Mater Sci Eng, A* 528:7933–7937
- [13] Zhao ZY, Guan RG, Guan XH et al (2015) Microstructures and properties of graphene–Cu/Al composite prepared by a novel process through clad forming and improving wettability with copper. *Adv Eng Mater* 7:663–668
- [14] Li M, Che H, Liu X et al (2014) Highly enhanced mechanical properties in Cu matrix composites reinforced with graphene decorated metallic nanoparticles. *J Mater Sci* 49:3725–3731. <https://doi.org/10.1007/s10853-014-8082-x>
- [15] Fadavi Boostani A, Tahamtan S, Jiang ZY et al (2015) Enhanced tensile properties of aluminium matrix composites reinforced with graphene encapsulated SiC nanoparticles. *Compos Part A Appl Sci* 68:155–163
- [16] Zhang Y, Li X (2017) Bioinspired, Graphene/Al₂O₃ doubly reinforced aluminum composites with high strength and toughness. *Nano Lett* 17:6907–6915
- [17] Zhang X, Li S, Pan D et al (2018) Microstructure and synergistic-strengthening efficiency of CNTs–SiCp dual-nano reinforcements in aluminum matrix composites. *Compos Part A Appl Sci* 105:87–96
- [18] Tang Y, Yang X, Wang R et al (2014) Enhancement of the mechanical properties of graphene–copper composites with graphene–nickel hybrids. *Mater Sci Eng, A* 599:247–254
- [19] Zhang D, Zhan Z (2016) Preparation of graphene nanoplatelets–copper composites by a modified semi-powder method and their mechanical properties. *J Alloy Compd* 658:663–671
- [20] Liu G, Zhao N, Shi C et al (2017) In-situ synthesis of graphene decorated with nickel nanoparticles for fabricating reinforced 6061Al matrix composites. *Mater Sci Eng, A* 699:185–193
- [21] Jiang C, Liu Z-K (2003) Computational investigation of constitutional liquation in Al–Cu alloys. *Acta Mater* 51:4447–4459
- [22] Zhang L, Wang J, Du Y et al (2009) Thermodynamic properties of the Al–Fe–Ni system acquired via a hybrid approach combining calorimetry, first-principles and CALPHAD. *Acta Mater* 57:5324–5341

- [23] Zhang X, Shi C, Liu E et al (2017) In-situ space-confined synthesis of well-dispersed three-dimensional graphene/carbon nanotube hybrid reinforced copper nanocomposites with balanced strength and ductility. *Compos Part A Appl Sci* 103:178–187
- [24] Zhang X, Shi C, Liu E et al (2017) Achieving high strength and high ductility in metal matrix composites reinforced with a discontinuous three-dimensional graphene-like network. *Nanoscale* 9:11929–11938
- [25] Qin J, He C, Zhao N et al (2014) Graphene networks anchored with Sn@graphene as lithium ion battery anode. *ACS Nano* 8:1728–1738
- [26] Zhou J, Qin J, Zhang X et al (2015) 2D space-confined synthesis of few-layer MoS₂ anchored on carbon nanosheet for lithium-ion battery anode. *ACS Nano* 9:3837–3848
- [27] Qin J, Wang T, Liu D et al (2018) A top-down strategy toward SnSb in-plane nanoconfined 3D N-doped porous graphene composite microspheres for high performance Na-Ion battery anode. *Adv Mater* 3:1704670
- [28] Yang M, Weng L, Zhu H et al (2017) Simultaneously enhancing the strength, ductility and conductivity of copper matrix composites with graphene nanoribbons. *Carbon* 118:250–260
- [29] Qu X, Wang F, Shi C et al (2018) In situ synthesis of a gamma-Al₂O₃ whisker reinforced aluminium matrix composite by cold pressing and sintering. *Mater Sci Eng, A* 709:223–231
- [30] Xin L, Yang W, Zhao Q et al (2017) Strengthening behavior in SiC nanowires reinforced pure Al composite. *J Alloy Compd* 695:2406–2412
- [31] Jiang L, Li Z, Fan G et al (2012) Strong and ductile carbon nanotube/aluminum bulk nanolaminated composites with two-dimensional alignment of carbon nanotubes. *Scr Mater* 66:331–334
- [32] Rashad M, Pan F, Tang A et al (2014) Effect of Graphene Nanoplatelets addition on mechanical properties of pure aluminum using a semi-powder method. *Prog Nat Sci* 24:101–108
- [33] Zhao L, Lu H, Gao Z (2015) Microstructure and mechanical properties of Al/Graphene composite produced by high-pressure Torsion. *Adv Eng Mater* 17:976–981
- [34] Li Z, Guo Q, Li Z et al (2015) Enhanced mechanical properties of graphene (reduced graphene oxide)/aluminum composites with a bioinspired nanolaminated structure. *Nano Lett* 15:8077–8083
- [35] George R, Kashyap KT, Rahul R et al (2005) Strengthening in carbon nanotube/aluminium (CNT/Al) composites. *Scr Mater* 53:1159–1163
- [36] Zhang H, Xu C, Xiao W et al (2016) Enhanced mechanical properties of Al5083 alloy with graphene nanoplates prepared by ball milling and hot extrusion. *Mater Sci Eng, A* 658:8–15
- [37] Chen B, Shen J, Ye X et al (2017) Length effect of carbon nanotubes on the strengthening mechanisms in metal matrix composites. *Acta Mater* 140:317–325
- [38] Fu K, Zhang X, Shi C et al (2018) An approach for fabricating Ni@graphene reinforced nickel matrix composites with enhanced mechanical properties. *Mater Sci Eng, A* 715:108–116
- [39] Hansen N (2004) Hall-Petch relation and boundary strengthening. *Scr Mater* 51:801–806
- [40] Chu K, Wang F, Li Y et al (2018) Interface and mechanical/thermal properties of graphene/copper composite with Mo₂C nanoparticles grown on graphene. *Compos Part A Appl Sci* 109:267–279
- [41] Munoz-Morris MA, Garcia-Oca C, Morris DG (2002) An analysis of strengthening mechanisms in a mechanically alloyed, oxide dispersion strengthened iron aluminide intermetallic. *Acta Mater* 50:2825–2836
- [42] Zhang D, Zhan Z (2016) Strengthening effect of graphene derivatives in copper matrix composites. *J Alloy Compd* 654:226–233